Digital Light Processing 3D Printing of Lightweight Fe_3O_4/rGO/resin Composites with Enhanced Microwave Absorption

Chenxing Xin [a], Jing Zhang [a], Ton Peijs [b], Yan Li [a*]

[a] Gemmological Institute, China University of Geosciences, Wuhan, 430074, PR China

[b] Materials Engineering Centre, WMG, University of Warwick, Coventry, CV4 7AL, UK

Corresponding author: yanli@cug.edu.cn

Abstract: A Fe_3O_4/rGO reinforced photocurable resin composite with gyroid structure was firstly fabricated by digital light processing (DLP) 3D printing. The obtained gyroid template was further coated with absorbants and experienced a post-curing treatment for microwave absorption (MA) applications. The minimum reflection loss of the Fe_3O_4/rGO/resin gyroid composite coated with Fe_3O_4/rGO nanoparticles reached -38 dB at 10.8 GHz and a thickness of 2.5 mm, while effective absorption band was 77% in the X-band, exhibiting the best MA performance. The leverage of DLP 3D printing allows for an optimal structure for absorbants coating and increases the opportunity for electromagnetic wave reflection/refraction/transmission. The synergistic effects of hybrid Fe_3O_4/rGO/resin template coated with Fe_3O_4/rGO and gyroid structure effectively promote the MA performance and realize the manufacturing of lightweighting composites for future electromagnetic protection applications.

Keywords: *3D printing, composite materials, digital light processing, Fe_3O_4/rGO, microwave absorption, gyroid structure.*

1. Introduction

With the rapid development of electromagnetic technology, the accompanying intensified electromagnetic pollution has drawn increasing attention [1]. Microwave absorption (MA) materials, with a wide absorption band and strong absorption ability, are promising materials for applications that need to shield and absorb the electromagnetic radiation and interface in undesired bandwidths [2]. Fe_3O_4 nanoparticles have been widely considered for their high magnetic saturation strength and magnetic loss ability, however, agglomeration in liquids and resins, and poor electrical conductivity greatly constrain its use in further applications [3, 4]. To tackle this problem, reduced graphene oxide (rGO) is currently being considered as an alternative choice in combination with Fe_3O_4 to enhance the electromagnetic MA performance of composites due to its high surface area, high charge carrier mobility, ultra-low density, and excellent electrical conductivity [5-7]. To date, some novel Fe_3O_4/rGO composite absorbers such as hierarchical porous Fe_3O_4/rGO [8], Fe_3O_4 flakes/rGO [9], and Fe_3O_4 hollow nanoflowers/rGO [10] with excellent MA performance have been successfully synthesized. However, these interesting MA materials still have seen limited applications due to their high weight and narrow absorption bandwidth [11]. Special design structures can make up for these drawbacks and have achieved excellent electric and magnetic loss properties, attributing to electromagnetic resonance and coupling effects [12, 13]. Due to the limitation of traditional material processing procedures (e.g., molding, hot-pressing, sintering and binding), only simple geometrical structures can be developed such as sandwich and honeycomb structures [14-16]. Digital light processing (DLP) 3D printing technology opens up new avenues to realize more complex structures with stronger MA performance, wider bandwidths and lightweighting by a combination of MA structure and material compositional design for higher resolution, precision, and customized complex designs. It adopts a layer-to-layer strategy with the projector – the designed pattern of each layer is projected, which improves the surface profile, surface roughness, and high printing efficiency [17].

In this study, Fe_3O_4/rGO nanoparticles fabricated via an *in-situ* reduction one-step solvothermal process were firstly DLP 3D printed using a photocurable resin. The printed gyroid structure acted as a template for maximum specific surface area, by regulating the infiltration of various absorbants in the template. The design of structure, material composition and absorbants coating allows for an enhancement in absorption bandwidth, reflection loss (R_L), and lightweighting, thus opening up potential applications in future MA devices.

2. Experimental

The synthesis process was illustrated in Fig. 1, 400 mg GO (JCNO Technology Co. Ltd, China, diameter: 0.5-3 μm, thickness: 1 nm, monolayer rate: ＞91%) was dispersed in ethylene glycol (EG, $C_2H_6O_2$, AR, 10009818) accompanied by ultrasonication treatment (Lawson DH92-IIN, China). 10 g $FeCl_3 \cdot 6H_2O$, 35 g NaAc powder and 5 g polyethylene glycol 1000 (PEG 1000) were dissolved into EG for 1 h by mechanical stirring to produce a yellow-brown liquid. Subsequently, the two mixtures were transferred into Teflon-lined stainless-steel autoclaves for solvothermal reaction at 180℃ for 12 h. The produced black precipitates were collected, washed, and dried.

The fabrication of photocurable resin (including a biodegradable PLA-PUA monomer, TEGDMA diluent and Irgacure 819 photoinitiator, in a 58:39:3 wt ratio) was reported in detail in our previous work [18]. The gyroid templates were DLP 3D printed using a 30 wt.% Fe_3O_4/rGO/resin suspension and further infiltrated in Fe_3O_4/rGO (50 wt.%) suspension and rGO suspension (4 wt.%), respectively, increasing the nanoparticle loading to 40 wt.% and 4 wt.%, respectively, after drying.

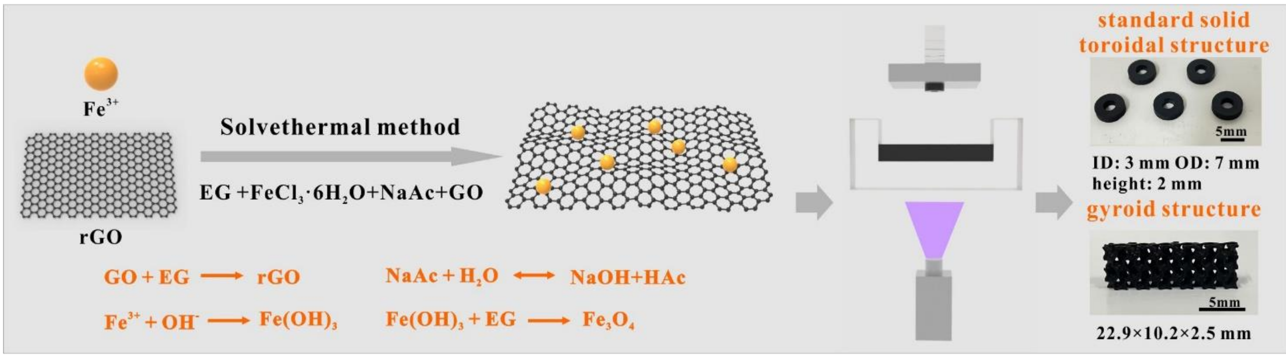

Fig. 1. Schematic of synthesis and DLP 3D printing process.

The morphology and structure of Fe_3O_4/rGO nanoparticles were characterized by transmission electron microscope (TEM, TF20). The 3D printed samples were measured by X-ray diffraction (XRD, D8 Advance 25), Raman spectroscopy (532 nm excitation laser, Horiba Scientific), and vibrating sample magnetometer (LakeShore7404). Electromagnetic parameters were measured by a vector network analyzer (VNA, Agilent E5071C), the printed toroidal samples were tested in the range of 1-18 GHz at room temperature (RT) using a coaxial method and the printed gyroid structures were tested in the range of 8.2 to 12.4 GHz (X-band) using a waveguide method.

3. Results and discussion

Spherical Fe_3O_4 nanoparticles were uniformly wrapped by 2D rGO nanosheets, producing multiple interfaces (Fig. 2a-b). Fig. 2c further shows an HRTEM image of Fe_3O_4/rGO, and the lattice fringes with an interplanar spacing value of 0.262

nm, related to the (311) planes of Fe_3O_4. Typical XRD diffraction peaks (Fig. 2d) of the 3D printed Fe_3O_4/rGO/resin composite at 18.28°, 30.06°, 35.45°, 37.12°, 41.04°, 53.55°, 57.17°, 62.73°, 70.78°, 74° and 79.08° reflected the cubic crystal structure of Fe_3O_4 (PDF 01-1111) [19], indicating that the crystal structure of Fe_3O_4 was successfully obtained in the solvent thermal method without damage induced to the crystal structure during the printing process. The absence of the rGO peak in the XRD pattern causing by the crystallization of Fe_3O_4 in the rGO interlayer destroyed the ordered interlayer structure of rGO. The magnetic behavior of neat resin (Fig. 2e) was almost a straight line, reflecting that there was no ferromagnetic behavior, while the hysteresis curve of the 3D printed Fe_3O_4/rGO/resin composite exhibited a typical S-like shape, with a saturation magnetization (M_S) value of 78.32 emu/g, indicating that it was superparamagnetic at RT. The Raman spectrum (Fig. 2f) detected a weak signal of rGO (D peak at 1353 cm^{-1}, G peak at 1588 cm^{-1}). The value of I_D/I_G indicated the disordering degree of the rGO, the ratio of the printed sample was 1.023, indicating that the graphitization of graphene was consistent with graphene made by Hummer's method after a reduction treatment [20].

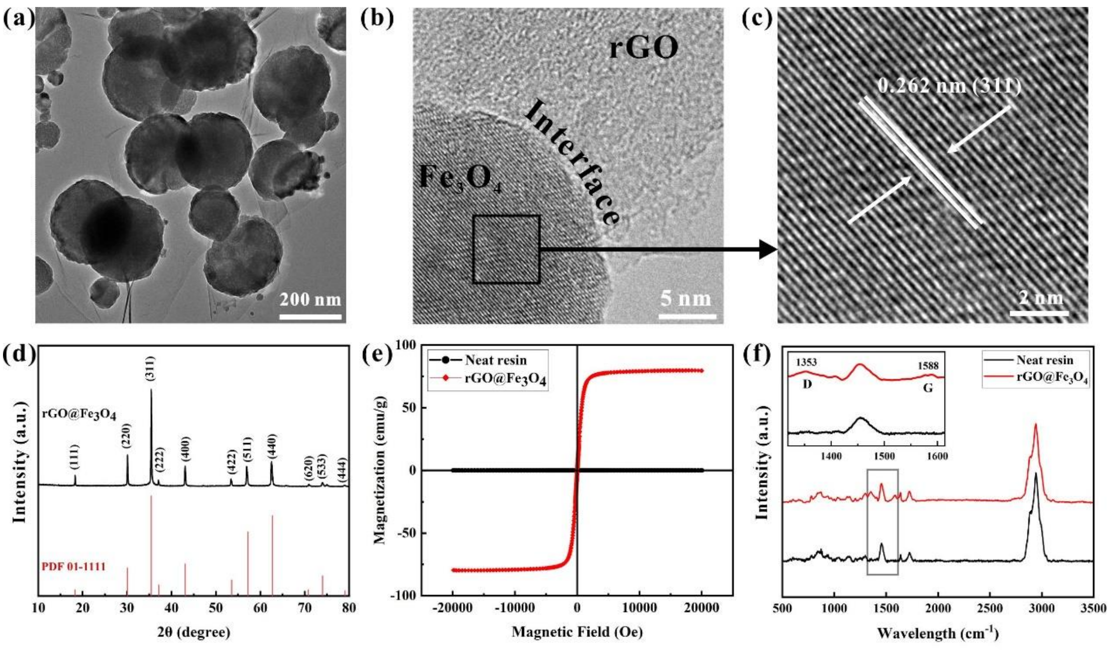

Fig. 2. (a-c) TEM images of synthesis of Fe_3O_4/rGO powder; (d) XRD patterns of the 3D printed the Fe_3O_4/rGO/resin composite; (e) RT magnetic hysteresis loops and (f) Raman spectrum of the 3D printed composite and neat resin.

With the addition of Fe_3O_4/rGO nanoparticles in resin, both the real part (ε', μ') and the imaginary part (ε'', μ'') values of complex permeability and permittivity of the printed Fe_3O_4/rGO/resin composite increased over the whole tested range

(Fig. 3a-b), which presented the storage ability of magnetic and electronic energy [21]. R_L value was adopted to evaluate the MA performance of the samples. Based on transmit-line theory, the R_L could be calculated by following equations: $Z_{in} = Z_0\sqrt{\frac{\mu_r}{\varepsilon_r}}\tan h[(j2\pi fd/c)\,(\mu_r\varepsilon_r)^{\frac{1}{2}}]$ and $R_L(\text{dB}) = 20\log\,|\frac{Z_{in}-1}{Z_{in}+1}|$.

Fig. 3c-d showed R_L values of DLP 3D printed neat resin and Fe_3O_4/rGO/resin composite of different thickness in the range of 1 to 18 GHz. The addition of Fe_3O_4/rGO greatly influenced the MA performance. The Fe_3O_4/rGO/resin composite had a minimum R_L (-26 dB at 4.73 GHz at a layer thickness of 5 mm), while the effective absorption bandwidth (<-10 dB) could reach 3.17 GHz (9.05-12.22 GHz) at a thickness of 2.5 mm. The attenuation ability of dielectric and magnetic absorption were described by the dielectric loss tangent ($\tan\delta_\varepsilon = \varepsilon''/\varepsilon'$) and magnetic loss tangent ($\tan\delta_\mu = \mu''/\mu'$) (Fig. 3e). Obviously both the dielectric and magnetic loss existed over the whole test range in the printed Fe_3O_4/rGO/resin composite, exhibiting typical magnetic resonance at 1-6 GHz, and the dielectric loss plays a more important role than magnetic loss in dissipating electromagnetic wave in the X-band ($\tan\delta_\varepsilon$= 0.21-0.34) [21, 22]. To further leverage the composites with excellent MA performance in the X-band, gyroid structures with a high surface area were printed as templates in a thickness of 2.5 mm (neat resin and Fe_3O_4/rGO/resin composite). There was no MA peformance improvement when using the neat resin as a template even coated with rGO or Fe_3O_4/rGO (Fig. 3f). In contrast, the Fe_3O_4/rGO/resin template infiltrated with Fe_3O_4/rGO suspension and post-cured displayed enhanced MA performance and a minimum R_L was reached at -22 and -38 GHz after infiltration with rGO and Fe_3O_4/rGO suspensions, respectively. It was also worth noting that the bandwidth exceeding -10 dB was 3.24 GHz (9.16-12.4 GHz), reaching 77% absorption band in the X-band after the Fe_3O_4/rGO/resin template was coated with Fe_3O_4/rGO, displaying the best MA performance compared with 30-40 wt.% Fe_3O_4/rGO composites (The mass fraction of powder in the paraffin wax) from literature (Fig. 3f). Fig. 3g further elaborates on the possible MA mechanism of composite with gyroid structure. Firstly, the introduction of a gyroid template structure increased the number of multiple reflections and scattering at the surface or inside the structure for microwaves. Secondly, the gyroid template provided a maximum surface area for nanoparticles coating, and this structural advantage effectively compensated for low concentration of graphene that could be introduced into photocurable resin due to the absorption of UV light. Thirdly, with the addition of Fe_3O_4/rGO nanoparticles, both the dielectric and magnetic loss ability are significantly enhanced, thereby favouring MA capability. Finally, the large number of rGO-rGO and rGO-Fe_3O_4 interfaces induced a strong interfacial polarization and associated relaxation effect, enhancing the attenuation capability of the composite and facilitates the conversion of electromagnetic energy into thermal energy.

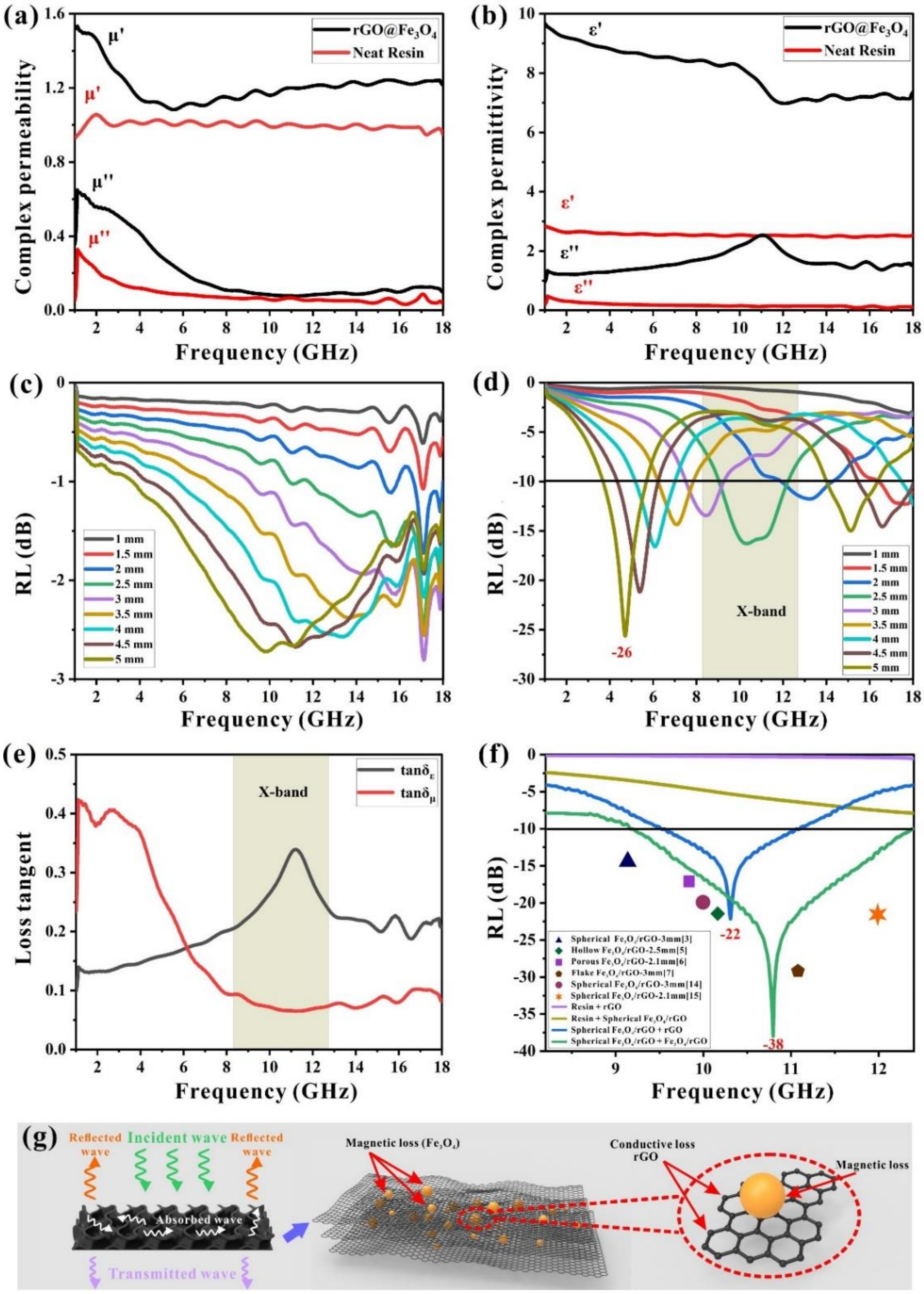

Fig. 3. (a) The complex permeability and (b) complex permittivity of Fe_3O_4/rGO/resin composite and neat resin with

toroidal structure; the R_L of (c) neat resin and (d) Fe_3O_4/rGO/resin composite; (e) loss tangent of Fe_3O_4/rGO/resin composite; (f) R_L values of the obtained composites and results from literature [4, 6, 9, 19, 20]; (g) Schematic diagram of MA mechanism.

4. Conclusion

A novel strategy was developed by leveraging a DLP 3D printed gyroid structure with the unique MA property of hybrid Fe_3O_4/rGO/resin composite with various absorbants coating to obtain a satisfactory absorption bandwidth in the X-band and enhanced MA performance, while simultaneously reducing thickness and realizing lightweight. The Fe_3O_4/rGO/resin gyroid template coated with Fe_3O_4/rGO nanoparticles displayed a minimum R_L of -38 dB at a thickness of 2.5 mm with an effective bandwidth (9.16-12.4 GHz), covering 77% in the X-band.

Acknowledgements

The work was financially supported by National Natural Science Foundation of China (No.51902295), Applied Basic Frontier Research of Wuhan Municipal Science and Technology Bureau (No.2019020701011454) and Hubei Province Natural Science Foundation grant (No. 2019CFB264).

Reference

[1] Y.X. Zuo, X.R. Su, X.W. Li, et al., Multimaterial 3D-printing of graphene/Li0.35Zn0.3Fe2.35O4 and graphene/carbonyl iron composites with superior microwave absorption properties and adjustable bandwidth, Carbon 167 (2020) 62-74, https://doi.org/10.1016/j.carbon.2020.05.071.

[2] Y. Zhao, L. Hao, X. Zhang, et al., A novel strategy in electromagnetic wave absorbing and shielding materials design: multi‐responsive field effect, Small Science 2(2) (2022) 2100077, https://doi.org/10.1002/smsc.202100077.

[3] A.K. Srivastava, B. Samaria, P. Sharma, et al., Electromagnetic wave absorption properties of reduced graphene oxide encapsulated iron nanoparticles, Mater. Lett. 253 (2019) 171-174, https://doi.org/10.1016/j.matlet.2019.06.011.

[4] J. Ren, L. Zhang, X. Fan, Rational self-assembly of Fe_3O_4 nanostructures on reduced graphene oxide for enhanced microwave absorption, J. Electron. Mater. 50(9) (2021) 5057-5071, https://doi.org/10.1007/s11664-021-09013-4.

[5] Y.C. Qing, D.D. Min, Y.Y. Zhou, et al., Graphene nanosheet- and flake carbonyl iron particle-filled epoxy-silicone composites as thin-thickness and wide-bandwidth microwave absorber, Carbon 86 (2015) 98-107, https://doi.org/10.1016/j.carbon.2015.01.002.

[6] Y. Zuo, Z. Yao, H. Lin, et al., Digital light processing 3D printing of graphene/carbonyl iron/polymethyl methacrylate nanocomposites for efficient microwave absorption, Compos. Pt. B-Eng 179 (2019) 107533, https://doi.org/10.1016/j.compositesb.2019.107533.

[7] G.H. Wang, Y. Zhao, F. Yang, et al., Multifunctional integrated transparent film for efficient electromagnetic protection, Nano-Micro Lett. 14(1) (2022) 65, https://doi.org/10.1007/s40820-022-00810-y.

[8] A.T. Pak, S.M. Masoudpanah, M. Adeli, et al., Hierarchical porous Fe_3O_4/RGO nanocomposite powders as high performance microwave absorbers, J. Mater. Res. Technol-JMRT 13 (2021) 548-560, https://doi.org/10.1016/j.jmrt.2021.05.002.

[9] S.Q. Jiao, M.Z. Wu, X.X. Yu, et al., Enhanced microwave absorption: The composite of Fe_3O_4 flakes and reduced graphene oxide with improved interfacial polarization, Adv. Eng. Mater. 22(4) (2020) 1901299, https://doi.org/10.1002/adem.201901299.

[10] X.J. Zeng, L.Y. Zhu, G.M. Jiang, et al., Template-free formation of uniform Fe_3O_4 hollow nanoflowers supported on reduced graphene oxide and their excellent microwave absorption performances, Phys. Status Solidi A-Appl. Mat. 215(7) (2018) 1701049, https://doi.org/10.1002/pssa.201701049.

[11] Y.H. Zhang, H.X. Si, S.C. Liu, et al., Facile synthesis of BN/Ni nanocomposites for effective regulation of microwave absorption performance, J. Alloys Compd. 850 (2021) 156680, https://doi.org/10.1016/j.jallcom.2020.156680.

[12] Y. Huang, X. Yuan, M. Chen, et al., Ultrathin flexible carbon fiber reinforced hierarchical metastructure for broadband microwave absorption with nano lossy composite and multiscale optimization, ACS Appl. Mater. Interfaces 10(51) (2018) 44731-44740, https://doi.org/10.1021/acsami.8b16938.

[13] Y. Duan, Q. Liang, Z. Yang, et al., A wide-angle broadband electromagnetic absorbing metastructure using 3D

printing technology, Mater. Des. 208 (2021) 109900, https://doi.org/10.1016/j.matdes.2021.109900.

[14] S.K. Singh, M.J. Akhtar, K.K. Kar, Impact of Al_2O_3, TiO_2, ZnO and $BaTiO_3$ on the microwave absorption properties of exfoliated graphite/epoxy composites at X-band frequencies, Compos. Pt. B-Eng 167 (2019) 135-146, https://doi.org/10.1016/j.compositesb.2018.12.012.

[15] Y. Gao, X.Y. Gao, J. Li, et al., Microwave absorbing and mechanical properties of alternating multilayer carbonyl iron powder-poly(vinyl chloride) composites, J. Appl. Polym. Sci. 135(12) (2018) 45846, https://doi.org/10.1002/app.45846.

[16] F. Wang, W.H. Gu, J.B. Chen, et al., The point defect and electronic structure of K doped LaCo0.9Fe0.1O3 perovskite with enhanced microwave absorbing ability, Nano Res. 15(4) (2022) 3720-3728, https://doi.org/10.1007/s12274-021-3955-1.

[17] C. Sun, N. Fang, D. Wu, et al., Projection micro-stereolithography using digital micro-mirror dynamic mask, Sens. Actuator A-Phys 121(1) (2005) 113-120, https://doi.org/10.1016/j.sna.2004.12.011.

[18] Z. Feng, Y. Li, C. Xin, et al., Fabrication of graphene-reinforced nanocomposites with improved fracture toughness in net shape for complex 3D structures via digital light processing, C-J. Carbon Res. 5(2) (2019) 25, https://doi.org/10.3390/c5020025.

[19] J.M. Wu, Z.M. Ye, W.X. Liu, et al., The effect of GO loading on electromagnetic wave absorption properties of Fe_3O_4/reduced graphene oxide hybrids, Ceram. Int. 43(16) (2017) 13146-13153, https://doi.org/10.1016/j.ceramint.2017.07.007.

[20] Y.P. Wang, Z. Peng, W. Jiang, Size-controllable synthesis of Fe_3O_4 nanospheres decorated graphene for electromagnetic wave absorber, Journal of Materials Science-Materials in Electronics 27(6) (2016) 6010-6019, https://doi.org/10.1007/s10854-016-4524-3.

[21] F. Wang, W. Gu, J. Chen, et al., Improved electromagnetic dissipation of Fe doping $LaCoO_3$ toward broadband microwave absorption, Journal of Materials Science & Technology 105 (2022) 92-100,

https://doi.org/10.1016/j.jmst.2021.06.058.

[22] L. Liang, W. Gu, Y. Wu, et al., Heterointerface engineering in electromagnetic absorbers: new insights and opportunities, Adv. Mater. 34(4) (2022) 2106195, https://doi.org/10.1002/smsc.202100077.